Molecular Therapy
Methods & Clinical Development
Original Article

Development of a scalable and robust AEX method for enriched rAAV preparations in genome-containing VCs of serotypes 5, 6, 8, and 9

Pranav R.H. Joshi,[1] Alice Bernier,[1] Pablo D. Moço,[1] Joseph Schrag,[2] Parminder S. Chahal,[2] and Amine Kamen[1]

[1]Viral Vectors and Vaccine Bioprocessing Group, Department of Bioengineering, McGill University, Montreal, QC, Canada; [2]Human Health Therapeutics, National Research Council of Canada, Montreal, QC, Canada

Removal of empty capsids from adeno-associated virus (AAV) manufacturing lots remains a critical step in the downstream processing of AAV clinical-grade batches. Because of similar physico-chemical characteristics, the AAV capsid populations totally lacking or containing partial viral DNA are difficult to separate from the desired vector capsid populations. Based on minute differences in density, ultracentrifugation remains the most effective separation method and has been extensively used at small scale but has limitations associated with availabilities and operational complexities in large-scale processing. In this paper, we report a scalable, robust, and versatile anion-exchange chromatography (AEX) method for removing empty capsids and subsequent enrichment of vectors of AAV serotypes 5, 6, 8, and 9. On average, AEX resulted in about 9-fold enrichment of AAV5 in a single step containing 80% ± 5% genome-containing vector capsids, as verified and quantified by analytical ultracentrifugation. The optimized process was further validated using AAV6, AAV8, and AAV9, resulting in over 90% vector enrichment. The AEX process showed comparable results not only for vectors with different transgenes of different sizes but also for AEX runs under different geometries of chromatographic media. The herein-reported sulfate-salt-based AEX process can be adapted to different AAV serotypes by appropriately adjusting elution conditions to achieve enriched vector preparations.

INTRODUCTION

Recombinant adeno-associated virus (rAAV)-based vectors have emerged as a platform of choice for therapeutic gene delivery in both dividing and non-dividing cells.[1,2] The clinical success and resulting regulatory approval of three rAAV-based drug products, namely Glybera, Luxturna, and Zolgensma, for single-dose curative gene therapy in hereditary monogenic disease indications have set new milestones.[3–5]

The progressive understanding of clinical and pharmacological implications of the presence of inadvertently co-synthesized empty capsids (ECs) in AAV lots during clinical studies opened new areas of investigation.[6] Devoid of a therapeutic transgene, these ECs do not exert direct clinical benefits. Many reports have suggested ECs' role in reducing transduction efficiency (while being in excess) through competition for receptor binding,[6] inducing dose-dependent capsid-neutralizing antibody response,[7] and cytotoxic T-lymphocyte-mediated destruction of transduced cells displaying capsid-associated peptide-MHC complexes.[8,9] On the other hand, a potential beneficial effect of excess ECs through their role as a decoy against immune response, protecting functional vector particles, has been suggested.[10] In this view, a resultant strategy proposed admixing sequence-modified, non-receptor-binding ECs of the same serotype in a precisely tailored ratio to a clinical lot of functional vector material (EC-free).[11] Importantly, in both scenarios, the removal of "co-existing" ECs remains a critical step. From a bioprocessing standpoint, the similarity in size and surface charge characteristics of these ECs with vector capsids (VCs) makes their removal challenging.

Ultracentrifugation (UC) approaches developed to remove ECs were based on density-gradient media such as cesium chloride or iodixanol, where ECs and VCs were separated based on their buoyant density.[12–14] Although large-scale UC has been industrially demonstrated in viral vaccine[15,16] and AAV vector purification,[17] the capital investment associated with this technology makes it difficult to implement in small and medium-size facilities. In parallel, various chromatographic protocols developed alone or in combination with UC to generate EC-free high-purity clinical-grade AAV material have been reviewed in detail and published.[18]

To further address UC-associated challenges, especially relevant in high-dose vector preparation for systemic administration (10^{12}–10^{14} viral genomes [VG]/kg)[19,20] and achieving an end-to-end linear scalability in the manufacturing process, multimodal chromatographic approaches emerged as a tool for overall downstream processing, including removal of ECs. These chromatographic protocols incorporate primary capture steps and intermediate purification steps of a specific modality[21–36] followed by an anion-exchange chromatography

Received 17 October 2020; accepted 18 March 2021;
https://doi.org/10.1016/j.omtm.2021.03.016.

Correspondence: Amine Kamen, Viral Vectors and Vaccine Bioprocessing Group, Department of Bioengineering, McGill University, Montreal, QC, Canada.
E-mail: amine.kamen@mcgill.ca

Table 1. Summary of affinity-purification process characteristics

Sample	VG/mL	Volume (mL)	Total VGs	VG recovery, %
AAV5-*gfp*/AVB sepharose[a,b]				
Feed	8.03×10^{10}	1,000	8.03×10^{13}	–
Flowthrough	3.07×10^{09}	1,000	3.07×10^{12}	3.82
Column wash	7.13×10^{08}	50	3.57×10^{10}	<1
Elution	6.72×10^{12}	10	6.72×10^{13}	83.69
AAV8-*gfp*/capture select AAVX[a,b]				
Feed	3.19×10^{10}	1,000	3.19×10^{13}	–
Flowthrough	5.47×10^{08}	1,000	5.47×10^{11}	1.71
Column wash	9.81×10^{07}	50	4.91×10^{09}	<1
Elution	2.61×10^{12}	10	2.61×10^{13}	81.82
AAV6-*gfp*/capture select AAVX[b]				
Feed	2.87×10^{10}	1,000	2.87×10^{13}	–
Flowthrough	7.24×10^{08}	1,000	7.24×10^{11}	2.52
Column wash	1.13×10^{08}	50	5.65×10^{09}	<1
Elution	2.33×10^{12}	10	2.33×10^{13}	81.18
AAV6-*cas9*/capture select AAVX[b]				
Feed	2.58×10^{10}	1,000	2.58×10^{13}	–
Flowthrough	5.44×10^{08}	1,000	5.44×10^{11}	2.11
Column wash	8.75×10^{07}	50	4.38×10^{09}	<1
Elution	2.15×10^{12}	10	2.15×10^{13}	83.33
AAV9-*gfp*/capture select AAVX[b]				
Feed	2.04×10^{9}	550	1.12×10^{12}	–
Flowthrough	1.16×10^{8}	550	6.40×10^{10}	5.7
Column wash	1.39×10^{8}	40	5.54×10^{9}	<1
Elution	8.8×10^{10}	10	8.8×10^{11}	78.23

VG, viral genomes analyzed via ddPCR.
[a]Average value for multiple runs (n = 3), relative SD < ± 10%.
[b]5 mL prepacked column.

(AEX) step for removal of ECs.[30,37–40] Moreover, anion-exchange protocols involving chromatography media with improved mass transfer, such as monolithic stationary phases[40] or adsorptive membranes, have also been reported.[39,41] These reports were specific to a particular serotype, such as AAV1,[39] AAV2,[42] AAV6,[43] and AAV8.[39–41] A recent report on VC enrichment of natural and engineered rAAV vectors from the affinity-purified preparations employing an AEX protocol demonstrated a step closer toward a generic AAV purification method.[30]

As part of our sustained efforts directed at improving AAV manufacturing technology, we report herein the development of a simple and scalable AEX protocol for removal of ECs and consequent enrichment of AAV5 VCs produced in insect-cell cultures. The generic nature of this AAV5-AEX protocol was further validated using AAV serotypes produced in mammalian cell cultures, demonstrating adaptability to different serotypes. Importantly, the discontinuous-gradient elution process, carefully tailored for each serotype, showed the robustness amenable to cGMP operation.

RESULTS

AAV sample preparation for AEX

In this study, immunoaffinity-purified AAV was used as a starting material. Besides providing high recovery in a single step, the affinity-purification step substantially increases the concentration of AAV and reduces the amount of non-AAV-related impurities. The immunoaffinity step recovery of genomic particles (VGs) for various AAV serotypes was found to be around 80%–85%, despite the starting lysate material originating from two different production platforms (insect-cell cultures and mammalian-cell cultures), containing different host-cell impurities. Table 1 shows a summary of overall recovery in flowthrough, wash, and eluted AAV collections during affinity-purification runs of insect-cell-produced AAV5-*gfp* and mammalian-cell-produced AAV6-*gfp*, AAV6-*cas9*, AAV8-*gfp*, and AAV9-*gfp*.

Screening of different salts and their effect on AAV5 elution profile in AEX

The prime task was to optimize the anion-exchange conditions such that the minute difference in net negative charge between AAV5 ECs and VCs can be exploited at a preparative scale. The screening of various mono (NaCl) and divalent (Na_2HPO_4 and Na_2SO_4) salts was conducted to understand the effect of the valence of the anionic counter-ions (chloride, monohydrogen phosphate, or sulfate) on the resolution and separation efficiency of AAV5 ECs over a continuous elution gradient. The affinity-purified AAV5 material was loaded onto an anion-exchange medium (CIMac AAV empty/full 0.1 mL, 1.3 μm pore diameter), and, after wash, it was subjected to a 20–420 mM linear salt concentration gradient over 200 column volumes (CV) (Figure 1). Each salt produced a distinct elution pattern where AAV5 particles eluted at low ionic strength, indicated as peaks 1 (ECs) and 2 (VCs) (Figure 1). The divalent salts not only provided better resolution of the two AAV-associated peaks but also displayed 260/280 nm absorbance ratios with values close to those representative of ECs and VCs (Table S1). Compared to NaCl, AAV5 elution at a lower salt concentration of divalent monohydrogen phosphate and sulfate indicate their higher displacement strength. Moreover, relative to NaCl, the peaks eluted with divalent salts were narrower and with less peak overlapping (Figure 1), suggesting improved enrichment and separation of VCs from ECs by divalent anions.

To account for the 3-fold difference in ionic strengths resulting from the different valences of the Cl^- and SO_4^{-2} ions, elution was studied by matching the ionic strength (IS) of the gradient and the slope. Based on the previous elution of AAV5 capsids in the range of 20–30 mM Na_2SO_4, the continuous gradient was run from 60–90 mM ionic strength at gradient slope adjusted to 2 mM IS/CV for both NaCl and Na_2SO_4. In the Na_2SO_4 gradient, the AAV5 capsids eluted at 60–90 mM ionic strength. In contrast, no AAV5 elution occurred in this range of the gradient in NaCl, where instead elution occurred at higher ionic strength (100–130 mM). The separation of EC and VC peaks in NaCl remained similar to that shown in Figure 1A.

The sulfate salt was selected over monohydrogen phosphate based on the relative ratio of signal intensity and absorbance peak area

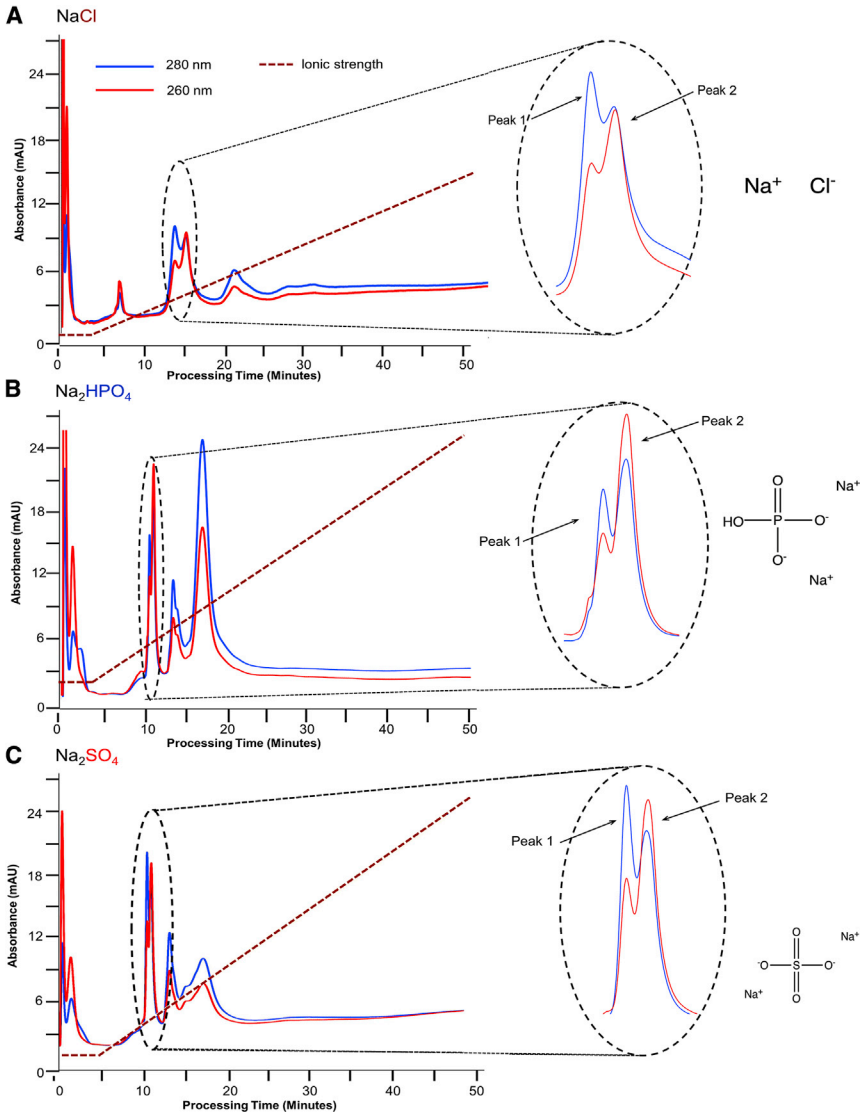

Figure 1. AAV5-*gfp* AEX elution profile under continuous gradient of different salts

The AEX column used in this study was a CIMac Q 0.1 AAV, processing buffer is 25 mM BTP (pH 9.0), and salt concentration gradient ranges from 20–420 mM in 200 CV with the slope of 2 mM salt/CV. The process flow rate was 0.5 mL/min. The magnified image of the AAV5 capsid peaks (peak 1 and 2), and corresponding salts' chemical structures are shown on the right-hand side. (A) AAV5-*gfp* elution in a NaCl continuous gradient. AAV5 capsid elution range is 100–130 mM. (B) AAV5-*gfp* elution in a Na_2HPO_4 continuous gradient with AAV5 eluting in the range of 25–35 mM. The larger AUP of the VC peak does not correlate with the VC proportion relative to ECs when compared with the *sv*-AUC profile of starting material. This indicates the co-elution of ECs in VC peak fraction. (C) AAV5-*gfp* elution in a Na_2SO_4 continuous gradient, where EC and VC peaks elute at a concentration range of about 20–30 mM. The 260/280 nm signal ratio closely corresponds with the known values of the EC and VC standards and *sv*-AUC results. AEX, anion-exchange chromatography; *sv*-AUC, sedimentation velocity analytical ultracentrifugation; AUP, area under the peak; CV, column volume; EC, empty capsid; VC, vector capsid.

at 260 nm and 280 nm for EC and VC peaks. For monohydrogen phosphate, the higher peak area of peak 2 compared to peak 1 indicated ECs being co-eluted with VCs (Table S1). The $A_{260/280}$ ratios and peak areas in sulfate were more representative of ECs and VCs, as confirmed by a comparative analysis of these peak areas against sedimentation velocity analytical UC (*sv*-AUC) profiles (Table S1).

Effect of chromatographic buffer composition and mode of operation

A pH screening study at pH 9.0, 9.5, and 10.0 was conducted to investigate its effect on the separation efficiency. No improvement in separation efficiency was observed above pH 9. Preparative scale process optimization was conducted on a fast protein liquid chromatography (FPLC) system employing a 1 mL scale AEX monolith column (CIMmultus QA 1 mL, 0.95–1.15 µm pore diameter) using bis-Tris propane (BTP) buffer (pH 9.0 ± 0.02) with 50 mM Na_2SO_4 salt in the elution buffer. A shallow continuous-gradient (0.66 mM IS/CV) process (Figure 2A), which efficiently separated EC and VC populations (Figure 2B), was developed. SDS-PAGE analysis of the eluted peak fractions (Figure 2C) confirmed that most AAV capsids eluted in peaks 1 and 2. Digital-droplet polymerase chain reaction (ddPCR) (Figure 2D; Table S2) and alkaline agarose gel analysis (Figure S1A) showed that the ECs eluted first in early elution fractions followed by VCs. Peak 3 and high-salt-wash fractions (100% B and 2 M NaCl wash) also contained residual AAV. From this continuous-gradient elution, a step-gradient elution process that resolved two capsid populations with operational simplicity was derived (Figure 2E). The *sv*-AUC analyses indicated 80% VCs and 20% ECs (Figure 2I) in the genomic peak fraction (Figure 2F), whereas the EC peak fraction showed over 95% ECs (Figure 2H). As a result, the VC content was enriched by ~9-fold from the initial ~9%, and EC content was reduced 4.5-fold from an initial ~91% (Figure 2G). It is notable that the relative proportion of the 79S population with respect to 95S also got reduced from 37% to 18% in the VC peak fraction. The summary of *sv*-AUC analyses expressed as fold improvement in VC enrichment is provided in Table 2. The calculation of the percentages of ECs and VCs from *sv*-AUC data of a representative AAV5 sample is demonstrated in the Supplemental calculations.

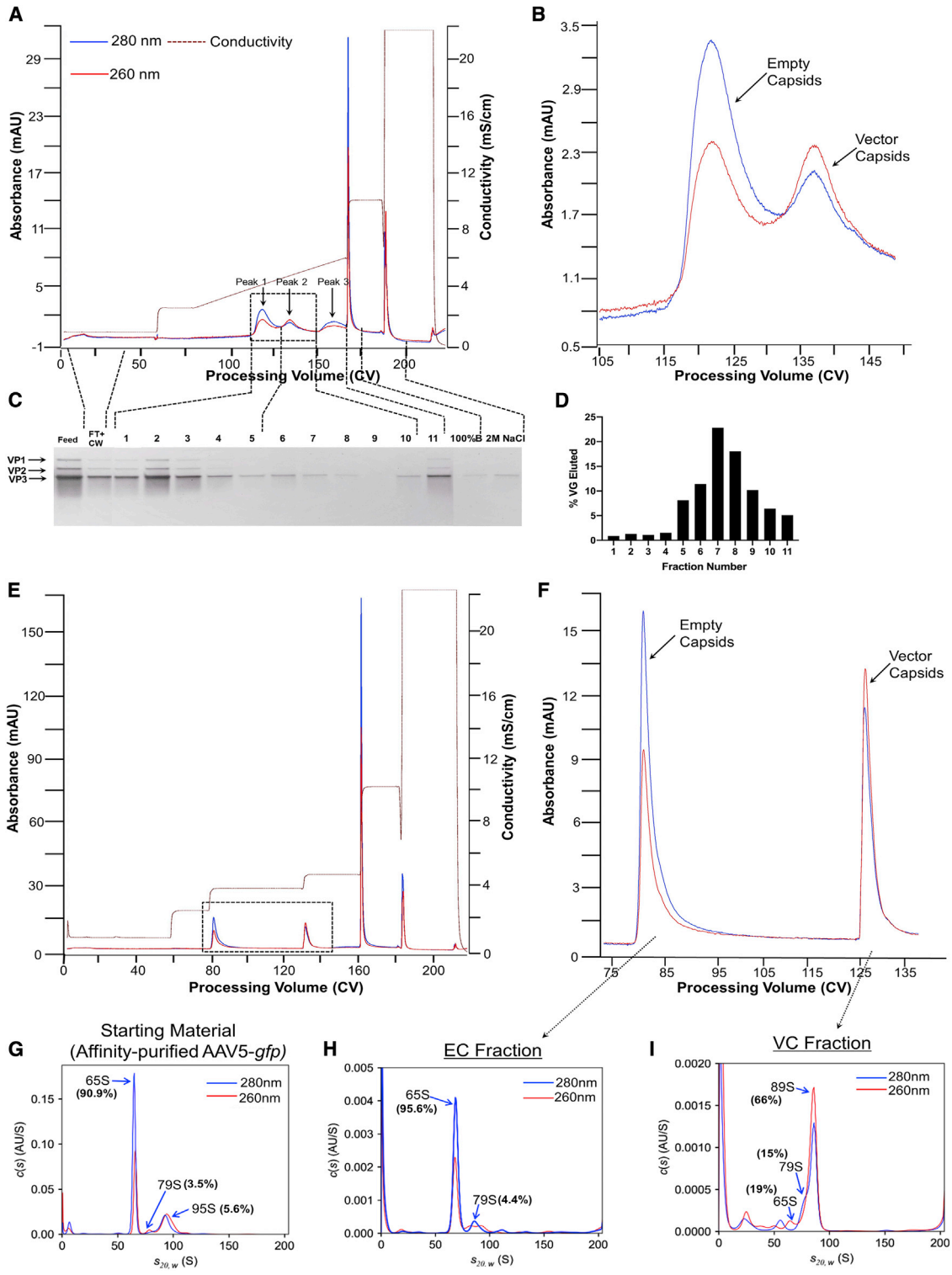

Figure 2. AAV5-*gfp* AEX process development

(A) AEX-process chromatogram of AAV5-*gfp* in a continuous gradient of elution buffer. Peaks eluting in this continuous gradient (peak 1, 2, and 3) and corresponding to AAV capsids are shown in a box. Multiple fractions were collected and analyzed by ddPCR to determine the presence of AAV capsids and packaged genome, respectively. (B)

(legend continued on next page)

Notably, the 95S VC population of the starting material (Figure 2G) appeared as an 89S population in the VC capsids (Figure 2I) collected in the AEX process. Interestingly, the packaged genome size was similar in both of these samples as analyzed via alkaline agarose gel electrophoresis (Figure 3D, AAV5-lanes 1 and 3). Although not clear, the higher S values (95S) could be due to the interaction of the VC population with other sample matrix components present in the affinity-purified material. The VC and EC contents of the same fractions were also analyzed by the optical-density measurement method,[44] and these results are in agreement with the *sv*-AUC results, as shown in Table 3. It should be noted that within the scope of this paper, the term VC refers to the entire population of AAV capsids encapsidating genomic material unless otherwise specified.

The VC fraction collected from the step-gradient run, when subjected to the second round of enrichment via continuous-gradient AEX run (Figures S1B–S1D), exhibited baseline separation of the residual EC population (~20%) from the VC population (Figure S1D), yielding a chromatographic profile resembling the *sv*-AUC profile (Figure S1E) of the VC peak fraction from a step-gradient elution (Figure S1B). This study further suggests that a near-complete removal of any residual ECs and additional VC enrichment can be effectively achieved via a second round of AEX run if needed.

AAV5 AEX-step reproducibility

For the reproducibility study, the affinity-purified AAV5 material from three different production runs was subjected to the AEX-step-gradient protocol. The *sv*-AUC profiles of VC peak fractions and graphical representation of reproducibility in VC enrichment from *sv*-AUC data are shown in Figures 3A and 3B. A lot-to-lot enrichment of samples in VCs with a relative standard deviation <5% was achieved.

Characterization of AEX-processed AAV5 lot

In addition to *sv*-AUC analysis, the purified and enriched VC preparations of AAV5 were analyzed for identity, purity, VP proteins ratio, and vector genome packaging using SDS-PAGE and alkaline agarose gel electrophoresis (Figures 3C and 3D). The SDS-PAGE profile confirms (1) EC and VC fractions with reduced protein impurities, and (2) three VP subunit proteins in a near prototypic ratio (1:1:10). The alkaline agarose gel electrophoresis profile also displayed two characteristics. First, in the EC fraction, a genome of <3 kb in size was detected in the form of a smear (Figure 3D, AAV5-*gfp*, lane 2), whereas the band(s) representing a large-size genome (>3 kb) was too faint to detect. Second, both a small-size genome (<3 kb) and a high-molecular-weight genome (3–4.5 kb) were present in the VC fraction (Figure 3D, AAV5-*gfp*, lane 3). The small genome (<3 kb) may represent fragments smaller than the vector expression cassette (3.8 kb), and the larger genome (>3.8 kb) may potentially represent co-packaging of other fragments with vector cassette.

The alkaline agarose gel electrophoresis results were also supported by the AUC profile of (1) EC fraction (Figure 2H), where the capsid population encapsidating small-size genome appeared as 79S peak; and (2) VC fraction (Figure 2I), which showed the presence of residual 79S capsids and capsids encapsidating large-size genome as 89S. Combined results of AUC and alkaline agarose gel electrophoresis suggest that AAV capsids encapsidating small-size intermediate genomic material co-eluted in the first EC fraction, and the remainder of these also eluted in VC fraction.

AEX-step generalization for AAV6, AAV8, and AAV9 serotypes

The AEX process generalization was studied by assessing its efficiency in the enrichment of VCs for other clinically relevant serotypes, AAV8, AAV9, and AAV6. We decided to use 10 mM BTP (pH 9.0) and sulfate salt with the monolith column. The affinity-purified material of serotypes AAV8 and AAV6 was first subjected to the continuous-gradient elution process (Figure S2) and, thereafter, a discontinuous-gradient process. Specific to serotypes, gradient step and buffer composition were adjusted to optimize the separation of ECs and VCs (Figure 4).

The sodium sulfate salt used for AAV5 was replaced with magnesium sulfate for AAV8. Magnesium sulfate offered slightly higher VC enrichment, as indicated by *sv*-AUC analysis of the VC peak fraction (Figures S3A and S3B). The magnesium sulfate salt was also used in the AAV6-AEX process, but initially AAV6 eluted as a single broad

Magnified image of AAV5 EC and VC capsid peaks eluted in a continuous gradient. (C) SDS-PAGE analysis of multiple fractions collected from a continuous-gradient run. Three bands corresponding to three VP subunits indicate the presence of the AAV capsid. Peak 3, 100% B, and 2 M NaCl fractions show the AAV VP bands, indicating residual AAV VC capsids eluted at high-salt-wash step. However, in contrast to AAV5 EC and VC fractions, these three fractions and the flowthrough fraction were required to be concentrated (~35×) before SDS-PAGE analysis to show a detectable signal. The high UV 280 nm signal in peak 3 may also indicate the co-elution of residual protein impurities present in the affinity-purified material. (D) VG analyses, via ddPCR, of multiple fractions collected from continuous-gradient run. A total of 13% VGs were detected in peak 1 (fractions 1–5), whereas around 70% of VG were detected in peak 2 (fractions 6–10). The presence of ~5% VGs in fraction 11 represents the elution of residual AAV VC capsids in peak 3 at the high-salt-wash (100% B) step. (E) AAV5-AEX chromatographic profile employing optimized process conditions (10 mM BTP and Na_2SO_4 as an eluent salt) of a step-gradient run. AAV5 EC and VC peaks are shown in a box. (F) Magnified image of AAV EC and VC peak fractions (as confirmed by SDS-PAGE and ddPCR). The first peak with AUP value for $A_{260/280}$ ratio of 0.58 corresponds to ECs, whereas the second peak with AUP value for $A_{260/280}$ ratio of 1.21 indicates predominantly the genome containing VCs. (G) *sv*-AUC profile of the affinity-purified AAV5-*gfp*. Three distinct AAV capsid populations with unique sedimentation coefficients were detected: (1) light capsids, 65S (ECs); (2) heavy capsids, 95S (VCs); and (3) intermediate population, 79S. The relative percentages of each of these AAV5 variants are 91% (65S), 3.5% (79S), and 5.5% (95S). (H) *sv*-AUC profile of AAV5 EC fraction. The dominant peak of ECs at 65S and a second small peak of intermediate species at 79S translate to their relative proportion of 95.6% and 4.4%, respectively. The absence of a peak at 95S indicates no detectable co-elution of VCs in this fraction. (I) *sv*-AUC profile of AAV5 VC fraction. The three distinct populations at 65S, 79S, and 89S have a relative proportion of ~19%, ~15%, and ~66%, respectively. ddPCR, digital-droplet polymerase chain reaction; VG, viral genome copies.

Table 2. Summary of VC enrichment via AEX

	Relative proportion, %					
	ECs	VCs				
Sample	Lighter capsids	Intermediate population	Heavier capsids	Fold VC enrichment	Relative ratio (ECs:VCs)	Relative ratio (heavier:intermediate capsids)
AAV5-*gfp*[a,b]						
	66S	79S	95S	–	–	–
Affinity-purified AAV5	90.91	3.43	5.66	–	10:1	1.6:1
EC peak fraction	95.6	4.4	ND	–	–	–
VC peak fraction	19.81	14.69	65.50 (89S)	8.8×	1:4	4.4:1
AAV8-*gfp*[a,b]						
	63S	74S	84S	–	–	–
Affinity-purified AAV8	62.56	2.03	35.41	–	1.7:1	17.4:1
EC peak fraction	96.6	ND	3.4	–	–	–
VC peak fraction	3.13[c]	4.22	92.65	2.6×	1:31	22:1
AAV6-*gfp*[d]						
Affinity-purified AAV6	63.17	36.83		–	1.7:1	–
EC peak fraction	93.28	6.72		–	–	–
VC peak fraction	5.36	94.64		2.6×	1:18	–
AAV6-*cas9*[d]						
Affinity-purified AAV6	60.59	39.41		–	1.5:1	–
EC peak fraction	95.72	4.38		–	–	–
VC peak fraction	4.54	95.46		2.4×	1:21	–
AAV9-*gfp*[d]						
Affinity-purified AAV9	67.63	32.37		–	2.1:1	–
EC peak fraction	94.96	5.04		–	–	–
VC peak fraction	5.28	94.72		2.9×	1:18	–

AEX, anion-exchange chromatography; EC, empty capsid; VC, vector capsid; ND, not detected.
[a]Average value for multiple runs (n = 3), relative SD < ± 5%.
[b]Values reported from *sv*-AUC analyses for determination of the relative proportion of ECs and VCs are based on 260 nm signal data.
[c]No visible peak of AAV8 63S was observed in AUC profiles of VC fraction (Figures 4E and 5A). In the sample with a very low UV signal, a small peak at 63S was observed (e.g., Figure 5A, lot #2). Although not clear if it was the noise of the UV detection, as the absorbance was below 0.001, calculations were made based on the UV signal peak area at this 63S position so as not to exclude the possibility of the 63S population present in trace amount.
[d]Values reported from the optical-density method for determination of the relative proportion of ECs and VCs.

peak (Figure S3C). The addition of 5 mM $MgSO_4$ to both the column equilibration buffer and the buffer-exchanged sample solved the problem of single-peak elution, and AAV6 ECs and VCs eluted as separate peaks in a continuous gradient (Figure S3D). The 5 mM salt supplementation strategy was ultimately applied to AAV5 (Na_2SO_4) and AAV8 ($MgSO_4$) as well. This additional salt supplementation helps retain components in flowthrough, which may otherwise bind in the absence of additional salt and elute at 5 mM salt.

The chromatograms of representative step-gradient AEX processes for AAV8 and AAV6 vectors and *sv*-AUC profiles of AAV8 EC and VC peak fractions are shown in Figure 4. The proportion of VC population (74S + 84S) in the VC peak fraction of AAV8 was increased to near 100% from the 37% observed in starting material as analyzed by *sv*-AUC (Figures 4A–4E), whereas no visible peak at 63S corresponding to AAV8 ECs was observed in this fraction. Comparable results were also obtained by the optical-density method (Table 3). Because of limited access to the AUC instrument and demonstrated comparability between *sv*-AUC and optical-density method determination of relative percentage ECs and VCs, the AAV6 samples were analyzed only by the latter method. Similar to AAV8, the final vector preparation of AAV6 also consisted of over 90% VCs (Table 2). The AEX process recovery and yield results for all serotypes are shown in Table S3.

Further characterization of AEX-processed lots via SDS-PAGE confirmed the purity of enriched VC fractions of AEX-purified AAV8-*gfp* and AAV6-*gfp*, which showed no major detectable protein impurities except a visible band of >250 kDa (Figure 3C). The alkaline agarose gel electrophoresis profiles of AAV8-*gfp* also showed the bands of <2 kb in size in the EC fraction (Figure 3D, AAV8-*gfp*, lane 2), indicating the co-elution of AAV8 capsids carrying small-

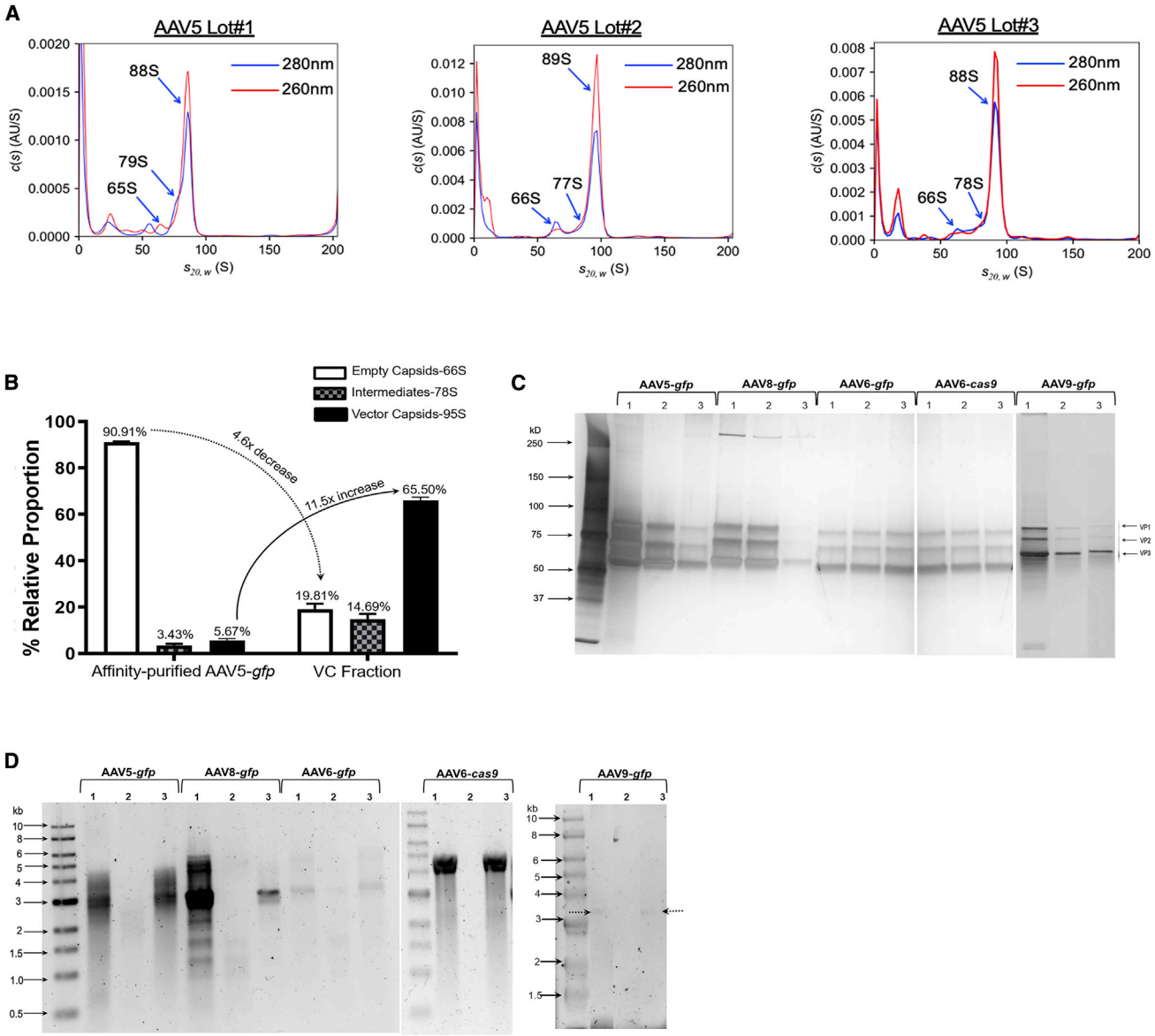

Figure 3. AAV5-AEX process reproducibility and characterization of AEX-processed AAV material

(A) *sv*-AUC profiles of OneBac/Insect cell produced AAV5 VC peak fractions collected from three different runs representative of three different production batches of AAV5. (B) Graphical representation of the AEX process reproducibility data for AA5-*gfp*. The individual column represents the percent relative proportion of ECs, VCs, and intermediate capsids determined from *sv*-AUC data of affinity-purified starting material and VC peak fractions. The VC peak fractions were collected from a representative optimized discontinuous gradient AEX process. The variability is represented by an error bar (RSD < 5%). (C) SDS-PAGE analysis of AEX-processed AAV fractions. Lanes 1, 2, and 3 correspond to the affinity-purified starting material, EC fraction, and VC fractions, respectively. For all serotypes, three major bands correspond to three VP subunits of AAV capsids. The gel image shows an absence of major protein impurities except that of >250 kDa in EC and VC (panel 2 and 3) fractions. (D) Alkaline agarose gel electrophoresis profile for vector genome analysis of AEX-processed AAV fractions. Lanes 1, 2, and 3 correspond to the affinity-purified starting material, EC fraction, and VC fractions, respectively. Notably, the size of the expression cassette (from ITR-to-ITR) for AAV5-*gfp*, AAV8/6-*gfp*, and AAV6-*cas9* is 3.79 kb, 2.9 kb, and 4.8 kb, respectively. (1) AAV5-*gfp*. In the case of affinity-purified AAV5-*gfp* sample (lane 1), the maximum packaged size is around 4.7 kb followed by a continuous smear between 3–4.5 kb, two visible bands around 3 kb and 2.8 kb, and finally a smear below 2.8 kb. In the EC fraction, a smear of size up to 2.4 kb is visible, indicating the presence of capsids packaging small-molecular-weight DNA. A similar trend is also visible as 79S intermediate capsid in the *sv*-AUC profile. In the VC capsid fraction (lane 3), similar to the affinity-purified sample, high-molecular-weight packaged DNA (3–4.5 kb), and low-molecular-weight DNA (<3 kb) are visible. (2) AAV8-*gfp*. In the case of the affinity-purified sample, the maximum packaged size for AAV8-*gfp* (lane 1) is around 5 kb, which is followed by a smear (3–5 kb) and multiple distinct bands <3 kb. In the EC fraction (lane 2), three bands <2 kb in size are visible, indicating the presence of capsids packaging small-size DNA. In the VC capsid fraction (lane 3), similar to the affinity-purified sample, high-molecular-weight DNA bands, a faint band at ~5 kb, and two dominant bands of 2.8 kb and 3 kb size are visible. Low signal intensities in this sample indicate a low sample amount compared to lane 1,

(legend continued on next page)

size intermediate genomic material. In the case of AAV6-*gfp*, the band of the size of the expression vector (2.9 kb), as well as smaller genome fragment (<2 kb), were detected in EC fraction (Figure 3D, AAV6-*gfp*, lane 2).

The AEX-step reproducibility, as demonstrated earlier for insect-cell-produced AAV5-*gfp*, was also assessed for HEK293-produced AAV8-*gfp* vectors. Three production lots of immunoaffinity-purified AAV8 vectors were subjected to the step-gradient AEX process (Figure 4A). The *sv*-AUC analysis of EC and VC fractions collected from these runs also showed a lot-to-lot reproducibility (Figures 5A and 5B) in VC enrichment with a variability of <5% relative standard deviation (RSD).

Further generalization of AEX-step

The versatility, herein defined as the ability of the AEX process to exhibit transgene-independent separation efficiency of ECs and VCs, was assessed for serotype-6-derived recombinant vectors. AAV6 was selected due to its reported potential in cell therapy and gene delivery applications.[45] An additional AAV6-*cas9* (4.8 kb) vector was selected for this study. The affinity-purified AAV6-*cas9* vector, when subjected to the AAV6-*gfp* AEX process (under both linear and step-gradient elution modes), eluted at the same salt ionic strength (% B steps) and showed EC and VC elution profiles identical to that of AAV6-*gfp* (Figures 4F, 4G, S1C, and S1D). Both quantitative (Table 2) and qualitative enrichment (Figures 3C and 3D) of AAV6-*cas9* VC were comparable to that of AAV6-*gfp*.

The AEX process developed for AAV8 was further assessed in a chromatography medium with a different resin matrix geometry and chemistry. The affinity-purified AAV8-*gfp* vector material was subjected to the same continuous-gradient AEX process using two different anion-exchange column configurations and matrices: monolith and packed bed. Notably, in both cases, the range of the salt gradient and its slope (1 mM IS/CV) were kept the same, whereas the flow rate was reduced from 10 mL/min on a monolith to 3 mL/min for packed bed to be within acceptable backpressure limits. Representative chromatograms of the AAV8-*gfp* purification are superimposed in Figure 5C. No substantial differences in the AAV8 EC and VC elution profiles and characteristics (Table S4) were observed.

A more basic capsid such as AAV9-*gfp* presented unique characteristics. In the conditions used for other strains (90% A + 10% B) and at 100% A, the AAV9 capsids did not bind to the CIMmultus QA column and remained in the flowthrough and column wash fraction, as confirmed with SDS-PAGE analysis of these fractions (Figures S4A and S4B). Next, AAV9 material was loaded onto the POROS HQ resin and found to bind in column equilibration condition with reduced salt (98% buffer A, 2% buffer B; Figure 5D). The bound AAV9-*gfp* capsids were first eluted under continuous-gradient elution followed by the development of a step-gradient elution protocol (Figure 5E). As expected, under a step-gradient elution protocol fine-tuned to achieve efficient separation between EC and VC populations, a highly enriched VC material exhibiting purity (Figure 3C) and packaged genome (Figure 3D) characteristics comparable to AAV6 and AAV8 was generated. Moreover, the $A_{260/280}$ ratio of 1.09 (Figure S4C) and VC proportion of more than 90% as analyzed via absorbance (Table 2) suggested comparable process performance.

DISCUSSION

The utilization of universal and highly effective UC-based protocols for large-scale AAV VC enrichment is limited by the availability, reservations to adapt and install, and operational feasibility in current GMP facilities for AAV production. Various GMP-amenable ion-exchange column chromatography protocols have also been reported to separate ECs and VCs based on minute differences in net capsid charges, obtaining varying degrees of VC enrichment. Many of these reported protocols were serotype-specific with limited application to other serotypes, and in recent times interest has grown in developing an AEX protocol that can be rapidly adapted to different serotypes to generate EC-free vector material. Aligned with this interest, in this paper we have reported a scalable anion-exchange chromatographic process for AAV5 VC enrichment with its adaptability demonstrated for other serotypes with minor adjustments.

During the salt-screening study, AAV5 elution in a continuous NaCl gradient displayed poor resolution and separation, with substantial overlapping between EC and VC peaks (Figure 1). Compared to monovalent chloride salt, the high-ionic-strength divalent anionic salts sodium monohydrogen phosphate (HPO_4^{-2}) and sodium sulfate (SO_4^{-2}) eluted AAV5 ECs and VCs with high-resolution separation of ECs and VCs (Figure 1), resulting in better VC enrichment as shown by $A_{260/280}$ ratio (Table S1). This observation was different from the previous AAV5-related publications, where the VC enrichment was achieved using either a weak anion exchanger (POROS PI) and a salt of monovalent chloride anions (KCl)[38] or a strong anion exchanger (POROS HQ) and salt of acetate (Tris-acetate)[30] or chloride (NaCl).[29,41] Better resolution and separation of AAV1 ECs and VCs on high-performance liquid chromatography (HPLC)-scale

which may be due to possible loss during the concentration step using centrifugal filters or low sample recovery after the *sv*-AUC run. The band at ~3 kb indicates the presence of capsids primarily and preferentially packaging complete vector (ITR-to-ITR). A trend similar to AAV8-*gfp* is also visible in (3) AAV6-*gfp* fractions, where, in the VC fraction (lane 3), a dominant band at ~3 kb indicates capsids with primarily packaging complete vector sequence. (4) AAV6-Cas9. In both affinity-purified (lane 1) and enriched VC fractions (lane 3), dominant high-molecular-weight DNA bands around 5 kb and 4 kb are visible, suggesting capsids preferentially packaging larger-size (high molecular weight) vector sequence. The faint smear below the 4 kb size indicates a continuum of intermediate capsid population packaging non-specific fragments of DNA. No visible band of small-molecular-size DNA in AAV6-*cas9* EC fraction may attribute to either their presence at the level below the LOD or absence in the sample. (5) AAV9-gfp. The alkaline agarose gel profiles of AAV9 feed and EC and VC fractions were similar to AAV8 and AAV8 vectors with the *gfp* cassette. ITR, inverted terminal repeats; LOD limit of detection; RSD, relative standard deviation,

Table 3. Comparability evaluation between *sv*-AUC and optical-density measurement for determination of relative percentage of ECs and VCs in purified AAV preparations

	sv-AUC analyses		Optical density method[44]	
Sample	ECs, %	VCs, %	ECs, %	VCs, %
Affinity-purified AAV5-*gfp*	90.91	9.09	89.71	10.29
AAV5-*gfp*/EC peak fraction	95.6	4.4	89.32	10.68
AAV5-*gfp*/VC peak fraction	19.81	80.19	10.57	89.43
Affinity-purified AAV8-*gfp*	62.56	37.44	61.07	38.93
AAV8-*gfp*/EC peak fraction	96.60	4.4	90.56	9.44
AAV8-*gfp*/VC peak fraction	3.13	96.87	4.37	95.63

sv-AUC, sedimentation velocity analytical ultracentrifugation; EC, empty capsid; VC, vector capsid.

column packaging analytical-grade nonporous 3 μm Mini Q beads was reported upon replacement of NaCl with kosmotropic salts of NH_4^+, PO_4^{-3}, and SO_4^{-2}.[46]

The intrinsic net negative charge differences of AAV5 ECs and VCs were exploited, employing a shallow elution gradient (0.66 mM IS/CV) of sodium sulfate salt, which resulted in improved resolution and separation compared to previous results. Although improved from the previous value of 0.49, the resolution coefficient of 0.77 was still less than ideal (>1.5), with reduced yet evident co-elution of ECs and VCs. The development of the step-gradient elution protocol was achieved via progressive improvements from a continuous-gradient run. The step changes were empirically applied and fine-tuned to understand the elution behavior and achieve the best possible separation efficiency, enrichment of VCs at a minimum cost of overall recovery. Our experience from the step-gradient protocol development suggests that the buffer B concentration at empty and genome capsid peak maxima in a shallow continuous-gradient run (0.66 mM IS/CV) offers a good starting point for a step change, which can be rapidly fine-tuned applying minimal adjustments.

A discontinuous (isocratic/step)-gradient elution protocol was thus developed, specifically tailored to ensure maximum EC removal, maximizing the VC enrichment and recovery. As a result of step optimization, substantial elution of ECs was achieved preceding the VC elution step. The partial co-elution of the intermediate population in both EC and VC (encapsidating full-length genome: ~4.7 kb) fractions indicated that its net negative charge lies between the two populations at the extremities. The VC elution step was also optimized to ensure minimum co-elution of contaminants (eluting just after the VC peak; Figure 2A, peak 3) present in the affinity-purified starting material. A slightly lower salt concentration step was selected to achieve this, which resulted in high purity and VC recovery (73%) at the expense of only 6% of VGs co-eluting in the later fractions with other contaminants. The collective recovery of the VGs in all fractions was above 90% (Table S3). SDS-PAGE analysis (after 35× concentration) showed that peak 3 had AAV VP components. However, this fraction did not show a significant proportion of VGs in ddPCR analysis (Figure 2D). This fraction may be composed of broken AAV capsid components (from low pH affinity elution), AAV aggregates, or other AAV capsid variants lacking packaged vector DNA.

The 80% AAV5 VC proportion in the step-gradient VC fraction as determined via *sv*-AUC analysis was comparable to the 82% (also analyzed via *sv*-AUC) recently reported by the team of Sanofi.[30] In both cases, despite different AAV5 production platforms and technology (One-Bac/Sf9 in our case and HEK293/triple plasmid transfection at Sanofi), the affinity-purified starting material consisted of approximately similar fractional content of ECs (91% in our case and 86% in the case of Sanofi) resulting in comparable fold reduction in ECs (~5×) after AEX-step. In other reports, the AAV5 VC content in the purified preparation was reported as 90%[38] or near 100%,[29] as determined from negatively stained transmission electron microscopy (TEM) analysis. The AEX-step recovery of 73% for AAV5 reported herein is higher than the previous reports of 6%[38] and 54%.[30]

The sulfate-based step-gradient elution approach initially developed for AAV5 was also successfully applied to gfp-expressing AAV6 and AAV8 vectors and Cas9-expressing AAV6 vector. For both serotypes, the step-elution profiles, VC enrichment (>90%), and recovery (80%–83%) were similar, demonstrating the versatility of the protocol independent of the serotype or the transgene. More than 95% VC proportion in AAV8-*gfp* preparation was comparable to previous AAV8 specific reports utilizing membrane anion-exchangers.[39,41] The AEX-step-gradient recovery of 81% is higher than the previous reports, where it was reported to be 43%[39] or 67%.[41] Similarly, for AAV6-*gfp*, the >90% VC proportion in the final preparation is comparable with the previous report.[30]

The monolith stationary phase is composed of a relatively uniform channel structure with dimensions sufficiently large to provide ready access to the ligand (binding site). The mass transfer is mainly driven by convective transport, whereas the effects of Eddies (random migration path) and pore diffusion limitations are minimized, offering better separation efficiency compared to packed-bed columns. In packed-bed columns, the overall mass transfer and separation efficiency are affected by all three means of mass transfer (convective transport, pore-diffusional limitation, and Eddie diffusion-random pathways). Overall, these geometrical differences between the two columns' formats may be responsible for different resolution coefficients (Table S4) and separation profiles (Figure 5C) achieved for a given serotype under the same buffer and gradient run conditions.

The earlier elution time (lower elution strength) in CIMmultus QA monolith can be potentially explained by the lower binding capacity resulting from a lower ligand amount and/or ligand density compared to POROS HQ resin. The reported dynamic binding capacity for BSA for both columns per the supplier's product information documents are ≥20 mg/mL for CIMmultus QA and 76–106 mg/mL for POROS

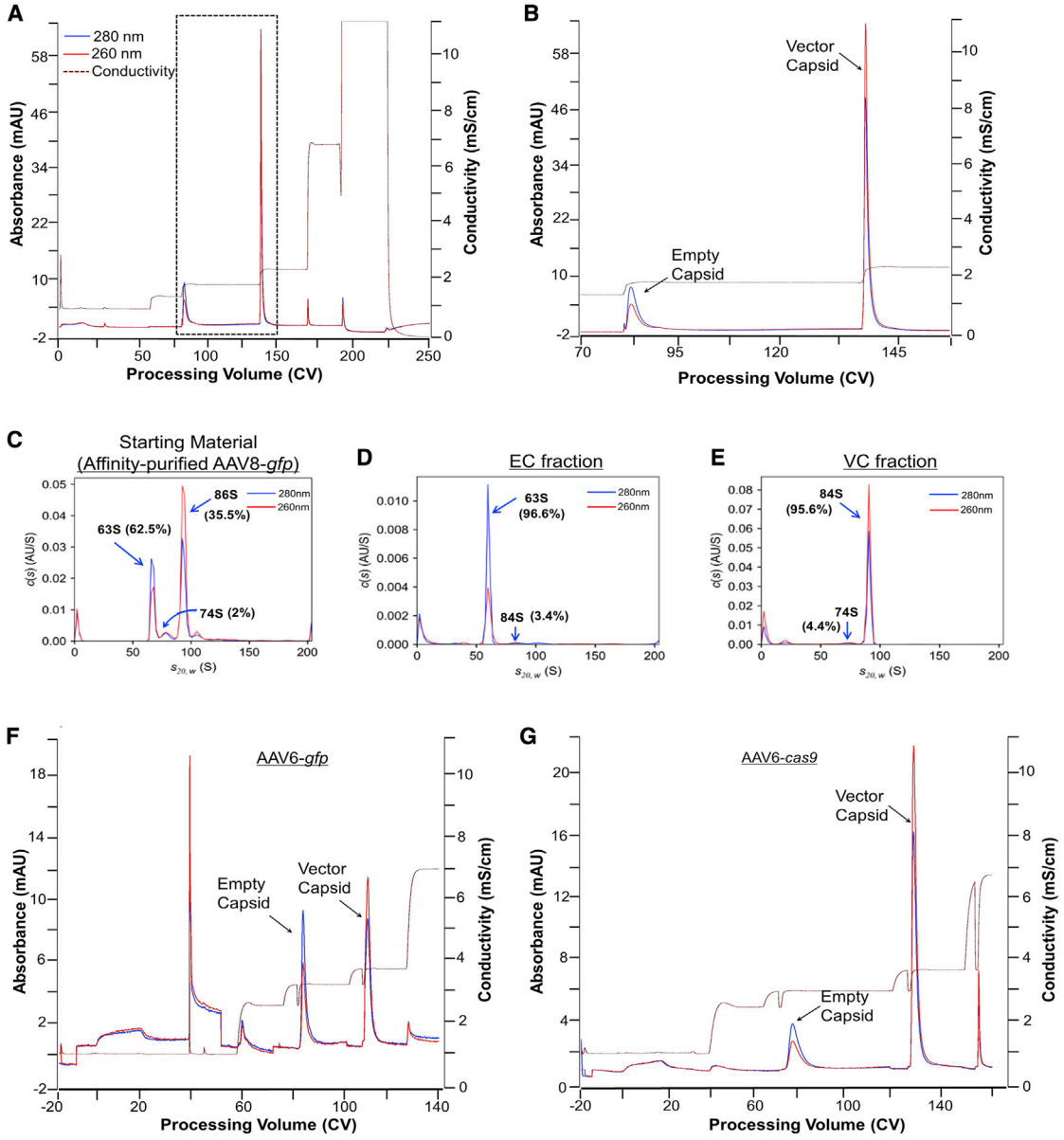

Figure 4. AAV-AEX process generalization demonstration for AAV6 and AAV8 serotype vectors

(A) AAV8 AEX chromatographic profile employing optimized process conditions of step-gradient AEX run. (B) Magnified image of two peaks corresponding to AAV8 capsids, as confirmed by SDS-PAGE and ddPCR. The first peak with $A_{260/280}$ ratio of 0.53 correlates to ECs, whereas the second peak with for $A_{260/280}$ ratio of 1.33 correlates to the genome-containing capsids. (C) *sv*-AUC profile of AAV8 starting material (affinity-purified AAV8-*gfp*). Three distinct AAV capsid populations with unique sedimentation coefficients are (1) light capsids, 63S (ECs); (2) heavy capsids, 86S (VCs); and (3) intermediate population, 74S. The relative percentages of each AAV8 capsid variant are 62.5% (63S), 2% (74S), and 35.5% (84S). Note the differential 260/280 nm signal profile for ECs and VCs, the intensities of which directly correspond to molar absorption coefficients of AAV8 capsid protein, packaged DNA, and their proportion. (D) *sv*-AUC profile of AAV8 EC fraction collected from a representative AEX run. The dominant peak of ECs at 63S and a small peak of VCs at 84S correlate to their relative proportion of 96.6% and 3.4%, respectively. (E) *sv*-AUC profile of AAV8 VC fraction. The two populations detected are intermediate species (74S) and heavy capsids-VCs (84S), with their relative proportion of 4.4% and 95.6%, respectively. (F and G) Step-gradient run profile employing optimized process conditions AAV6-*gfp* (F) and AAV6-*cas9* vectors (G). The higher 260 nm signal intensity in the VC peak of AAV6-*cas9* (G) compared to AAV6-*gfp* (F) potentially corresponds to the difference in the molar absorption coefficients due to different size vector DNA (*gfp*-2.9 kb Vs. *cas9*-4.8 kb).

HQ. This suggests that the ligand amount and/or ligand density in POROS HQ is higher, offering more binding capacity and stronger binding. As a result, higher salt concentration (higher ionic strength or conductivity) is required for elution, resulting in later elution times from POROS HQ compared to CIMmultus QA in equivalent gradients. These data suggest that AAV8 capsids remain bound to POROS

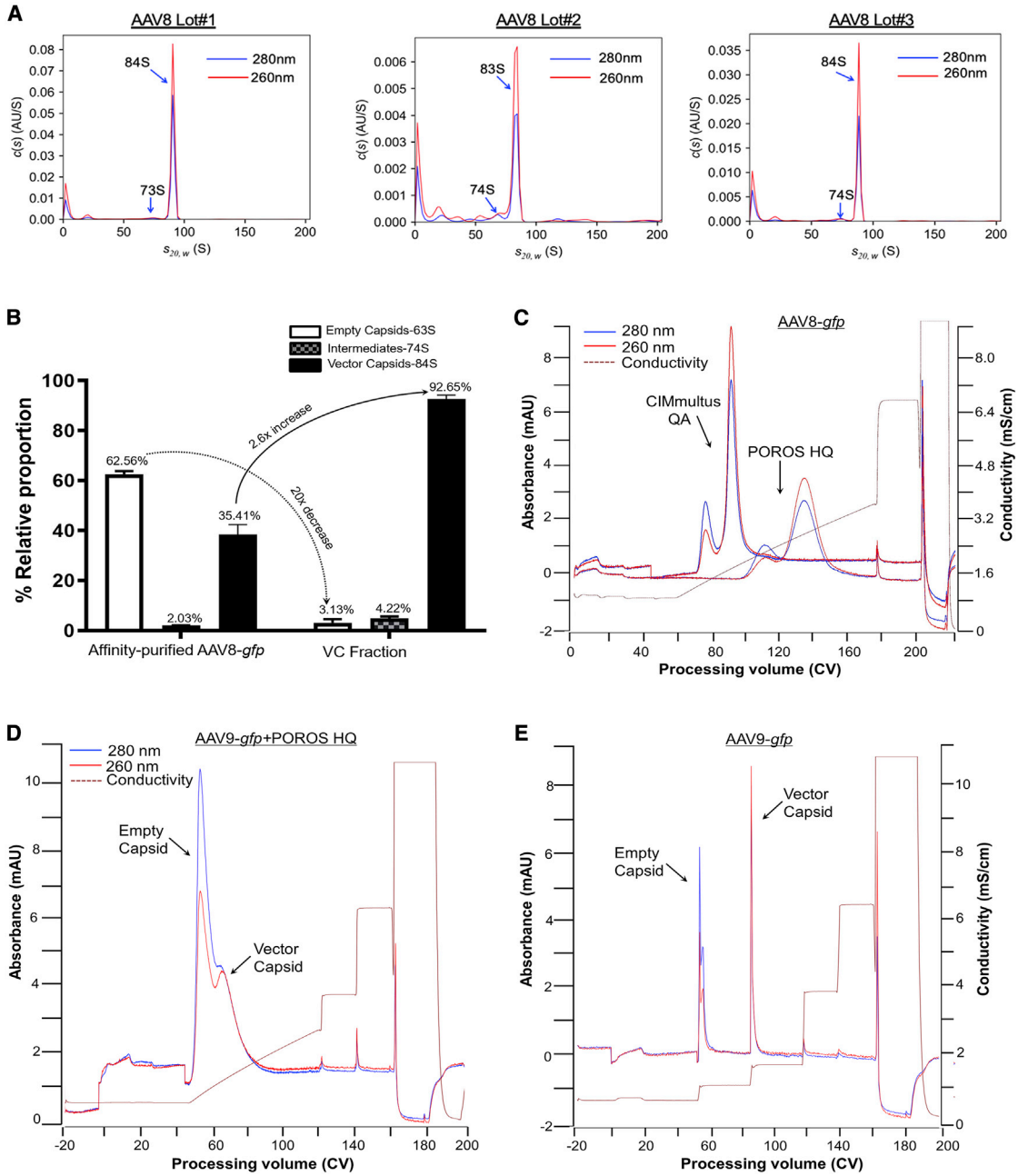

Figure 5. AEX-step reproducibility and adaptability demonstration for AAV8-*gfp* vectors

(A) *sv*-AUC profiles of HEK293SF cell produced AAV8-*gfp* VC peak fractions collected from three different production batches of AAV8, demonstrating reproducible enrichment. (B) Graphical representation of the AEX process reproducibility data AA8-*gfp*. Each plot represents the relative % proportion of ECs, VCs, and intermediate capsids determined from *sv*-AUC data for starting material and VC peak fractions. The VC peak fractions were collected from a representative optimized discontinuous gradient AEX process. The variability is represented by an error bar (RSD < 5%). (C) Superimposed chromatographic elution profiles of AAV8-*gfp* AEX run using monolith (CIMmultus QA-1 mL) and packed bed (POROS HQ-1 mL) under $MgSO_4$ salt gradient from 20–120 mM ionic strength over 100 CV. In the case of monolith column, AAV8 ECs and VCs eluted at 36.5 mM and 50.5 mM ionic strengths, whereas, in the case of packed-bed column, ECs and VCs eluted at higher ionic strengths of 65.5 mM and 87.5 mM, respectively. (D and E) AEX continuous-gradient elution profile (D) and optimized step-gradient elution profile (E) of AAV9-*gfp* using the POROS HQ column. Note the low elution strength of AAV9 capsids (<2 mS/cm conductivity) in a step-gradient run.

HQ resin at the salt condition, where it elutes from CIMmultus QA column. Higher ligand density on the POROS HQ compared to the CIMmultus QA matrix is likely to explain the observed differences in binding of AAV9 capsids. Moreover, this further suggests that AAV9 capsids are relatively basic in nature and exert less net negative charge (more positive charge) at pH 9 buffer conditions as compared to other serotypes tested in this study.

Process scale limitations in our academic lab precluded performing scale-up studies. However, the formats of the chromatography media used in this study (monolith and packed bed) are readily scalable. Packed-bed chromatography has been in regular use for biopharmaceutical manufacturing at various scales, including pilot and commercial-scale production. Commercial scale-up using monolith is in development for AAV-based gene therapy medicine.[47] Given the similar hydrodynamic (channel size and hence the porosity) and thermodynamic (ligand density, dynamic binding capacity) characteristics across different scales (Table S5), an easy and readily implementable scale-up of our reported process with appropriate adjustments in flow rate and loading conditions (AAV capsids/mL of column) can be expected.

It was observed that the efficiency of chromatographic resolution of ECs and VCs under continuous elution gradient and consequent VC enrichment in a step-gradient process was inversely related to the relative proportion of ECs in the affinity-purified starting material. The EC and VC peak resolution of the AAV5 sample containing 90% EC fractional content was lower (R_s: 0.77) than the AAV8 or AAV6 (R_s: 1.1–1.3) sample having 65% of fractional EC content. Similar to peak resolution, the consequent enriched VC content (% VC) in a step-gradient process was also lower for AAV5 (81% VC) compared to AAV6 or AAV8 (>90% VC). These findings are also in agreement with the previous report, where AAV5 VC enrichment was reportedly as high as 100% when the starting material consisted of 55% of ECs as opposed to the AAV5 starting material with 86% ECs, which resulted in 82% of VCs post-single-step AEX.[30] Both these reports suggest that further VC enrichment may be achieved with an additional AEX cycle by removing any residual ECs as demonstrated for AAV5 if needed (Figures S1C and S1D). Moreover, while comparing the efficiency of different chromatographic VC enrichment processes, the fractional content of ECs and VCs in both starting and enriched material should be considered for an accurate evaluation.

For AAV8, $MgSO_4$ provided slightly better VC enrichment than Na_2SO_4 (Figures S2A and S2B). Given that the anion is the same, that indicates that the cation (Na^+) plays some role in the separation. In the case of AAV6, 5 mM $MgSO_4$ salt supplementation was found to be a prerequisite for EC and VC separation in the form of two peaks (Figure S2), suggesting a potential interaction with the AAV6 capsid. Similarly, better separation and enrichment of AAV6[43] and AAV2[48] VCs was reported when 2 mM magnesium salt ($MgCl_2$) was supplemented into the elution buffer. We found VC enrichment for AAV5 using $MgSO_4$ to be inferior compared to that achieved with Na_2SO_4 (data not shown).

The exact mechanism of AEX-based separation of AAV ECs and VCs is not yet clear. Although competitive displacement is a well-recognized elution model in general,[49–53] the potential role of salt-induced charge neutralization and/or conformational change in the AAV capsids should not be overlooked. Further investigation on the interaction of salts with genome-less AAV ECs and genome-encapsidating VCs would be useful to better understand the separation mechanism.

Employing various AAV characterization techniques, including *sv*-AUC/optical-density analyses, ddPCR, SDS-PAGE, and alkaline agarose gel analysis, we have demonstrated that the step-elution protocol using sodium or magnesium sulfate salt can efficiently generate preparations highly enriched in AAV VCs and can be potentially applied to multiple AAV serotypes. A schematic representation of the overall manufacturing process flow is depicted in Figure 6. Similar elution profiles of AAV8 capsids under the shallow continuous-gradient run in both monolith and packed-bed resin columns indicate that our AEX process can be readily adapted to two widely used chromatography media without requiring significant changes. We have also demonstrated the effectiveness of this protocol for serotypes produced in two widely used platforms for commercial manufacturing of AAV vectors.

MATERIALS AND METHODS

Cell culture and baculovirus

Stably transformed *rep2cap5* packaging Sf9 cells (B8) and suspension adapted mammalian cells (HEK293SF) used for rAAV viral vector production were provided by Dr. Zolotukhin (University of Florida, Gainesville, FL, USA) and Dr. Chahal (National Research Council of Canada, Montreal, QC, Canada), respectively. The Sf9/B8 and HEK293SF-cells were maintained in serum-free suspension cultures at appropriate cell-culture conditions (27°C for Sf9 and 37°C, 5% CO_2, and 85% relative humidity for HEK293 cells) in a shaker incubator (Infors, Basel, Switzerland) at 120 rpm speed of agitation. The maintenance and production medium for insect cells and mammalian cells were Sf900-II (Thermo Fisher Scientific, Waltham, MA, USA) and Hycell TransFx-H (Cytiva Life Sciences, Chicago, IL, USA) (additionally supplemented with 0.1% w/v of Kolliphor P188 and 4 mM Glutamax), respectively. The cell density analysis for routine maintenance flasks and virus production run was performed using the Vi-Cell XR cell counter (Beckman Coulter, Brea, CA, USA). The recombinant baculovirus carrying the AAV transgene expression cassette (Bac-*gfp*) consisted of an AAV2-ITR flanking *egfp* under the control of chicken β-actin-CMV hybrid promoter. The recombinant baculovirus stock used for rAAV5 production was generated using naive Sf9 cells following a standard protocol, as published in our previous report.[54]

Recombinant AAV vector production

AAV5 production in insect cells and AAV6 and AAV8 production in HEK293SF cells was carried out applying baculovirus infection and triple-plasmid transient transfection protocols, respectively, as previously reported.[54,55] In brief, for AAV5 production, B8 Sf9 cells were

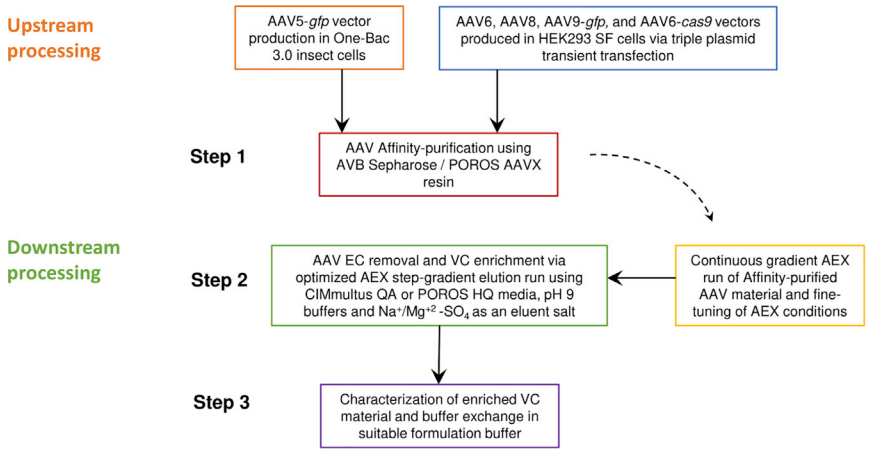

Figure 6. Schematic representation overall AAV manufacturing process-flow incorporating two-step chromatographic approach

AAV produced in insect cells via baculovirus expression vector platform or in HEK239 cells via triple-plasmid transient-transfection process are primarily recovered via cell culture harvest and cell lysis. The clarified cell lysate containing AAV is then subjected to the AAV immunoaffinity capture chromatography, where bound AAVs are collected via low pH elution. This purified mixture of AAV ECs and VCs is first subjected to the continuous gradient AEX, followed by the fine-tuning of step-elution gradients. Enriched VC material collected from optimized step-elution gradient AEX process is characterized and finally buffer-exchanged in a suitable formulation buffer.

infected with Bac-GFP baculovirus at a MOI of 3 in high cell-density (~10 million cells/mL) fed-batch suspension cultures. The cell culture was provided with nutrient feed formulation in pre- and post-baculovirus infection phases at specific time points.[54] For AAV6 and AAV8 productions, the HEK293SF cells at 1–1.2 million cells/mL were transiently transfected using 5% v/v PEI:DNA complex at a ratio of 2:1. The final concentrations of plasmid DNA and PEI (catalog number 23966-1, Polysciences, Warrington, PA, USA) were 1 μg/mL and 2 μg/mL of cell culture, respectively. The three plasmids used for AAV production were as follows: (1) pAdDeltaF6-helper (a gift from James M. Wilson, catalog number 1128677, Addgene, Watertown, MA, USA), (2) Rep2Cap-6/-8/-9 (Provided by Dr. Samulski, University of North Carolina, Chapel Hill, NC, USA), and (3) pAAV-CAG-GFP (a gift from Edward Boyden, catalog number 37825, Addgene, Watertown, MA, USA) or pAAV-PGK-saCas9-U6-sgRNAsa (catalog number C306, Applied Biological Materials, Richmond, BC, Canada). The AAV production scale was 1 L and 3 L cell culture for AAV5/Sf9 and AAV-6, -8, and -9/HEK293SF, respectively.

Culture harvest, primary recovery, and affinity purification

The insect cells and mammalian cells were harvested at 72 h post-infection and 48 h post-transfection, respectively. The insect cells were harvested through an *in situ* whole broth cell lysis protocol, whereas the mammalian cells were harvested by cell pellet lysis. In both cases, the cell culture or the cell pellets were mixed with lysis buffer such that the final concentration of buffer components was 50 mM Tris-HCl (pH 7.5), 0.1% Triton X-100, 2 mM $MgCl_2$, and 50 U/mL of Benzonase DNase (Millipore Sigma, Burlington, MA, USA). The cell lysate was incubated with lysis buffer at 37°C for 2 h, followed by the addition of $MgSO_4$ to increase the overall ionic strength of the lysate to 600 mM with an additional half-hour incubation before the clarification step. The lysate was clarified using an Optiscale capsule filter consisting of a Milligard membrane-1.2/0.5 μm (catalog number SWSCA47HH3, Millipore Sigma, Burlington, MA, USA). The clarified lysate was then subjected to a single-step affinity capture chromatography using commercially available 5 mL pre-packed immunoaffinity resin columns, AVB Sepharose (Cytiva Life Sciences, Chicago, IL, USA) for AAV5 or CaptureSelect AAVX (Thermo Fisher Scientific, Waltham, MA, USA) for AAV6 and AAV8. The affinity purification process was conducted on the ÄKTA Avant25 FPLC system. The affinity-resin-bound AAVs were eluted in 0.1 M glycine (pH 2.5) and were immediately neutralized via addition of 10% v/v of 1 M Tris (pH 8.8). The neutralized AAV material was buffer-exchanged into a suitable buffer using PD-10 desalting columns (Cytiva Life Sciences, Chicago, IL, USA). The linear flow rate of the process was 75 cm/h, providing 2 min residence time. The pH, conductivity, and UV-Vis absorbance were monitored throughout the process.

AEX for AAV genome-containing capsid enrichment

The salt screening study was conducted using an analytical-scale anion-exchange monolith column (CIMac AAV empty/full 0.1 mL, 1.3 μm pore diameter) on the Waters Alliance HPLC system. The affinity-purified AAV5 material was buffer-exchanged in 25 mM bis Tris propane, pH 9 buffer, and injected onto the column. The bound AAV5 capsids were eluted under a continuous salt gradient of elution buffers containing specific eluent salt (NaCl or Na_2HPO_4 or Na_2SO_4) at 0.5 mL (5 CV)/min flow rate. For preparative scale AEX processing, the affinity-purified AAV material was buffer-exchanged into the AEX column equilibration buffer before loading. The anion-exchange chromatography medium used was either monolithic (CIMmultus QA 1mL) or packed bed (POROS HQ-50 μm beads, 1 mL). The buffers were: (A) 10 mM BTP (pH 9.0); (B) 10 mM BTP (pH 9.0) + either 50 mM Na_2SO_4 (AAV5) or 50 mM $MgSO_4$ (AAV6 and AAV8); and (C) 2 M NaCl. The chromatographic steps in a continuous-gradient elution process were as following: equilibration: 90% A + 10% B (20 CV), (for AAV9: 98% A + 2% B); sample loading: (10 CV); column wash-1: 90% A + 10% B (30 CV); elution: 10% B → 50% B (150 CV) (for AAV9: 2% B → 25% B); column wash-2: 100% B (20 CV); and column wash-3: 100% C. The process flow rate for the monolith column run was 10 mL/min, and for the

packed-bed column it was 3 mL/min. Derived from the continuous elution gradient was the discontinuous (step)-gradient process. The column equilibration and column wash 1, 2, and 3 steps were as indicated above. The finalized discontinuous-gradient steps for elution of ECs and VCs of various AAV serotypes were as follows: (1) AAV5 EC (37.5% B) and VC (46% B), (2) AAV8 EC (15.5% B) and VC (23% B), (3) AAV6 EC (35% B) and VC (43% B), and (4) AAV9 EC (7% B) and VC (15% B). The elution step (% B) for ECs was selected such that it will ensure a maximum EC elution without significant co-elution of VCs (and hence without significant loss of VCs) before the next step applied to elute VCs. The UV signal returning to the baseline for each step was achieved by appropriately adjusting the step-gradient length, ensuring the near-complete elution of a given component. Additional column-wash steps before and after the AAV capsid elution were added to remove impurities, as indicated above. The AEX-process runs, conducted on the ÄKTA Avant25 FPLC system, were monitored using inline pH, conductivity, and UV-VIS sensors.

Process reproducibility study

Three individual vials from a working cell bank of packaging insect cells (*rep2cap5* Sf9) B8 or HEK293SF were used. Three different lots of recombinant baculovirus or plasmid stock were used at the upstream processing stage to produce three batches of AAV5 or AAV8 vectors. The AAV5 or AAV8 material generated was then subjected to affinity chromatography and AEX-steps. All chromatographic runs were carried out on different days, involving different lots of freshly prepared chromatography processing buffers for each run.

Quantification of DNase-resistant genomic particles (VG) by ddPCR

The clarified lysate or chromatography processed material was incubated with 5 U/mL of Benzonase for 30 min at 37°C before viral DNA extraction. Benzonase-treated samples both undiluted and 1:10 diluted were used for viral DNA extraction using a High Pure Viral DNA Extraction kit (Roche Diagnostics, Risch-Rotkreuz, Switzerland). The ddPCR assay was conducted using the QX200 Digital Droplet PCR system (Bio-Rad Laboratories, Hercules, CA, USA) as per the manufacturer's instructions. The reaction mixture for the AAV5-*gfp* sample consisted of a forward primer (5′-ATAGGGACTTTCCATTGA CGTC-3′), a reverse primer (5′- TGATACACTTGATGTACTGCC AAG-3′), and a probe (FAM 5′-TGGGTGGACTATTTACGGT AAACTGCC-3′ BHQ) targeting the CMV enhancer sequence. For AAV6/AAV8-*gfp*, the reaction mixture consisted of a forward primer (5′-CTGCTGCCCGACAACCAC-3′) and a reverse primer (5′-TCAC GAACTCCAGCAGGAC-3′) designed to target the transgene (EGFP) sequence. The primer set for AAV6-*cas9* vector is as follows: forward primer (5′-GGCCAGATTCAGGATGTGCT-3′) and reverse primer (5′-CATCATCCACAGAAGCGTGT-3′). The primers and a probe were purchased from Integrated DNA Technologies (Coralville, IA, USA). The thermocycling temperature programming for AAV5-*gfp* (preincubation at 95°C/15 min for denaturation and 40 cycles of 95°C/15 s and 54.5°C /30 s) and AAV6-/AAV8-/AAV9-*gfp* (preincubation at 95°C/15 min for denaturation and 40 cycles of 94°C/30 s and 60°C /1 min) were optimized explicitly for specific primers set.

sv-AUC analyses

For AUC analyses, the samples from affinity purification or AEX process fractions containing AAV capsids were buffer-exchanged into PBS and concentrated using Amicon Ultra (Millipore Sigma, Burlington, MA, USA) centrifugal filter with a 30 kDa molecular weight cut-off. The concentrated sample was then analyzed using a Beckman Proteomelab XL-1 ultracentrifuge (Beckman Coulter, Brea, CA, USA). The centerpieces were charcoal filled-epon, two-sector centerpieces with a 1.2 cm pathlength. The reference sector was filled with 420 μL PBS and the sample sector with a concentrated AAV sample. Samples were temperature equilibrated at 20°C with a full vacuum applied for 1 h. The sedimentation analysis run was performed at 20,000 rpm for 2 h at 20°C using absorbance detection at 260 and 280 nm. Data analysis was performed using Sedfit.[56] The data visualization plots were created using Gussi freeware.[57]

SDS-PAGE analysis

AEX process fractions were used for the analysis of purity and identity of components via SDS-PAGE. The concentrated elution fractions or concentrated samples recovered after *sv*-AUC analysis were subjected to denaturing protein electrophoresis run conditions. After the run, the gel was stained using Silver Stain Plus (Bio-Rad Laboratories, Hercules, CA, USA) as per supplier's instructions and visualized using the ChemiDoc Imager (Bio-Rad Laboratories, Hercules, CA, USA).

Alkaline agarose gel electrophoresis

The concentrated elution fractions or concentrated samples recovered after *sv*-AUC analysis were subjected to alkaline agarose gel electrophoresis. The recovered sample was mixed with 6× alkaline loading buffer (180 mM NaOH, 6 mM EDTA, 18% Ficoll 400, 0.15% bromophenol blue, and 0.25% xylene cyanol) in 6:1 proportion to get the final concentration of alkaline loading buffer to 1×. The alkaline running buffer comprises 30 mM NaOH and 2 mM EDTA in Milli-Q water. The 0.7% agarose gel was prepared by dissolving agarose powder in the alkaline running buffer. 30 μL of samples and 10 μL of Quick-Load 1 kb DNA ladder (New England Biolabs, Ipswich, MA, USA) in 1× alkaline loading buffer were loaded on the gel and run at 3.5 V/cm for extended hours until the dye had migrated approximately 2/3 the length of the gel. Post electrophoresis, the gel was washed with 0.5 M Tris-HCl (pH 8) buffer for 30 min and was incubated with staining buffer (1× SYBR Safe stain in TE buffer [pH 8]) for 1 h, followed by gel imaging using the ChemiDoc Imager.

SUPPLEMENTAL INFORMATION

Supplemental information can be found online at https://doi.org/10.1016/j.omtm.2021.03.016.

ACKNOWLEDGMENTS

P.R.H.J. is financially supported through a grant from the Natural Sciences and Engineering Research Council (NSERC RGPIN-2015-05132) of the government of Canada. A.K. is a recipient of a Canada

Research Chair (CRC/240394). The authors thank Alina Venereo-Sanchez for providing ready-to-use AAV9 plasmids and AAV9-*gfp* lysate material. The authors would like to thank Aleš Štrancar (BIA separation) for providing a gift sample of monolith anion-exchange columns, Mehul Patel (National Research Council of Canada, Montreal, QC, Canada) for providing a gift sample of POROSHQ prepacked 1 mL column, and Orjana Terova and Alejandro Baccera (Thermo Fisher Scientific) for providing gift samples of CaptureSelect AAVX resin and prepacked columns for preliminary studies. The authors would also like to thank Marie-Hélène Venne (National Research Council of Canada, Montreal, QC, Canada) for providing a protocol for vector genome analysis.

AUTHOR CONTRIBUTIONS

Conceptualization, P.R.H.J., P.S.C., and A.K.; design of experiments, P.R.H.J., A.B., J.S., P.S.C., and A.K.; chromatographic process development, P.R.H.J.; AAV production and characterization, P.R.H.J., J.S., and P.D.M.; writing – original draft, P.R.H.J.; writing – review & editing, P.S.C., A.B., J.S., and A.K.; funding acquisition, A.K.; resources, P.S.C., J.S., and A.K.; supervision, P.S.C. and A.K.

DECLARATION OF INTERESTS

The authors declare no competing interests.

REFERENCES

1. Huang, S., and Kamihira, M. (2013). Development of hybrid viral vectors for gene therapy. Biotechnol. Adv. *31*, 208–223.
2. Waehler, R., Russell, S.J., and Curiel, D.T. (2007). Engineering targeted viral vectors for gene therapy. Nat. Rev. Genet. *8*, 573–587.
3. Ylä-Herttuala, S. (2012). Endgame: glybera finally recommended for approval as the first gene therapy drug in the European union. Mol. Ther. *20*, 1831–1832.
4. Spark Therapeutics (2017). FDA advisory committee briefing document. Spark Therapeutics, Inc. Luxturna (voretigene neparvovec). Meeting of the cellular tissue, and gene therapies advisory committee. October 12, 2017.
5. Byrnes, A. (2019). ZOLGENSMA. Summary basis for regulatory action. Office of the tissue and advanced therapies signatory authority. May 24, 2019.
6. Wright, J.F. (2014). AAV empty capsids: for better or for worse? Mol. Ther. *22*, 1–2.
7. Mingozzi, F., and High, K.A. (2007). Immune responses to AAV in clinical trials. Curr. Gene Ther. *7*, 316–324.
8. Li, H., Lasaro, M.O., Jia, B., Lin, S.W., Haut, L.H., High, K.A., and Ertl, H.C.J. (2011). Capsid-specific T-cell responses to natural infections with adeno-associated viruses in humans differ from those of nonhuman primates. Mol. Ther. *19*, 2021–2030.
9. Mingozzi, F., Maus, M.V., Hui, D.J., Sabatino, D.E., Murphy, S.L., Rasko, J.E.J., Ragni, M.V., Manno, C.S., Sommer, J., Jiang, H., et al. (2007). CD8(+) T-cell responses to adeno-associated virus capsid in humans. Nat. Med. *13*, 419–422.
10. Hoffman, B.E., and Herzog, R.W. (2013). Covert warfare against the immune system: decoy capsids, stealth genomes, and suppressors. Mol. Ther. *21*, 1648–1650.
11. Martino, A.T., Basner-Tschakarjan, E., Markusic, D.M., Finn, J.D., Hinderer, C., Zhou, S., Ostrov, D.A., Srivastava, A., Ertl, H.C.J., Terhorst, C., et al. (2013). Engineered AAV vector minimizes in vivo targeting of transduced hepatocytes by capsid-specific $CD8^+$ T cells. Blood *121*, 2224–2233.
12. Ayuso, E., Mingozzi, F., Montane, J., Leon, X., Anguela, X.M., Haurigot, V., Edmonson, S.A., Africa, L., Zhou, S., High, K.A., et al. (2009). High AAV vector purity results in serotype- and tissue-independent enhancement of transduction efficiency. Gene Ther. *13*, 419–422.
13. Mueller, C., Ratner, D., Zhong, L., Esteves-Sena, M., and Gao, G. (2012). Production and discovery of novel recombinant adeno-associated viral vectors. Curr. Protoc. Microbiol. *Chapter 14*, 1–21.
14. Zolotukhin, S., Byrne, B.J., Mason, E., Zolotukhin, I., Potter, M., Chesnut, K., Summerford, C., Samulski, R.J., and Muzyczka, N. (1999). Recombinant adeno-associated virus purification using novel methods improves infectious titer and yield. Gene Ther. *6*, 973–985.
15. Morita, M., Aizawa, M., Toi, H., Fukuhara, E., and Hashimoto, K. (2011). Continous flow ultracentrifuge system for production of infection prevention vaccines. Hitachi Review. *60*, 257–261.
16. Reimer, C.B., Baker, R.S., Van Frank, R.M., Newlin, T.E., Cline, G.B., and Anderson, N.G. (1967). Purification of large quantities of influenza virus by density gradient centrifugation. J. Virol. *1*, 1207–1216.
17. Meriño, S.F., and Haifeng, C. (2016). International patent WO 2016/114991 A2, International filing date: 08/01/2016, International Publication date: 21/07/2016.
18. Qu, W., Wang, M., Wu, Y., and Xu, R. (2015). Scalable downstream strategies for purification of recombinant adeno- associated virus vectors in light of the properties. Curr. Pharm. Biotechnol. *16*, 684–695.
19. Wells, D.J. (2017). Systemic AAV gene therapy close to clinical trials for several neuromuscular diseases. Mol. Ther. *25*, 834–835.
20. Galibert, L., and Merten, O.W. (2011). Latest developments in the large-scale production of adeno-associated virus vectors in insect cells toward the treatment of neuromuscular diseases. J. Invertebr. Pathol. *107* (*Suppl*), S80–S93.
21. Auricchio, A., O'Connor, E., Hildinger, M., and Wilson, J.M. (2001). A single-step affinity column for purification of serotype-5 based adeno-associated viral vectors. Mol. Ther. *4*, 372–374.
22. Auricchio, A., Hildinger, M., O'Connor, E., Gao, G.P., and Wilson, J.M. (2001). Isolation of highly infectious and pure adeno-associated virus type 2 vectors with a single-step gravity-flow column. Hum. Gene Ther. *12*, 71–76.
23. Zolotukhin, S., Potter, M., Zolotukhin, I., Sakai, Y., Loiler, S., Fraites, T.J., Jr., Chiodo, V.A., Phillipsberg, T., Muzyczka, N., Hauswirth, W.W., et al. (2002). Production and purification of serotype 1, 2, and 5 recombinant adeno-associated viral vectors. Methods *28*, 158–167.
24. Smith, R.H., Levy, J.R., and Kotin, R.M. (2009). A simplified baculovirus-AAV expression vector system coupled with one-step affinity purification yields high-titer rAAV stocks from insect cells. Mol. Ther. *17*, 1888–1896.
25. Anderson, R., Macdonald, I., Corbett, T., Whiteway, A., and Prentice, H.G. (2000). A method for the preparation of highly purified adeno-associated virus using affinity column chromatography, protease digestion and solvent extraction. J. Virol. Methods *85*, 23–34.
26. Harris, J.D., Beattie, S.G., and Dickson, J.G. (2003). Novel tools for production and purification of recombinant adeno-associated viral vectors. Methods Mol. Med. *76*, 255–267.
27. Koerber, J.T., Jang, J.H., Yu, J.H., Kane, R.S., and Schaffer, D.V. (2007). Engineering adeno-associated virus for one-step purification via immobilized metal affinity chromatography. Hum. Gene Ther. *18*, 367–378.
28. Potter, M., Chesnut, K., Muzyczka, N., Flotte, T., and Zolotukhin, S. (2002). Streamlined large-scale production of recombinant adeno-associated virus (rAAV) vectors. Methods Enzymol. *346*, 413–430.
29. Brument, N., Morenweiser, R., Blouin, V., Toublanc, E., Raimbaud, I., Chérel, Y., Folliot, S., Gaden, F., Boulanger, P., Kroner-Lux, G., et al. (2002). A versatile and scalable two-step ion-exchange chromatography process for the purification of recombinant adeno-associated virus serotypes-2 and -5. Mol. Ther. *6*, 678–686.
30. Nass, S.A., Mattingly, M.A., Woodcock, D.A., Burnham, B.L., Ardinger, J.A., Osmond, S.E., Frederick, A.M., Scaria, A., Cheng, S.H., and O'Riordan, C.R. (2017). Universal method for the purification of recombinant AAV vectors of differing serotypes. Mol. Ther. Methods Clin. Dev. *9*, 33–46.
31. Gao, G., Qu, G., Burnham, M.S., Huang, J., Chirmule, N., Joshi, B., Yu, Q.-C., Marsh, J.A., Conceicao, C.M., and Wilson, J.M. (2000). Purification of recombinant adeno-associated virus vectors by column chromatography and its performance in vivo. Hum. Gene Ther. *11*, 2079–2091.

32. Chahal, P.S., Aucoin, M.G., and Kamen, A. (2007). Primary recovery and chromatographic purification of adeno-associated virus type 2 produced by baculovirus/insect cell system. J. Virol. Methods *139*, 61–70.

33. Zhou, A. (2010). International patent WO 2010/148143 Al, filed June 16, 2010, and published December 23, 2010.

34. Zhou, J., Yang, X., Wright, J.F., High, K.A., Couto, L., and Qu, G. (2011). PEG-modulated column chromatography for purification of recombinant adeno-associated virus serotype 9. J. Virol. Methods *173*, 99–107.

35. O'Riordan, C.R.O., Lachapelle, A.L., Vincent, K.A., and Wadsworth, S.C. (2000). Scaleable chromatographic purification process for recombinant adeno-associated virus (rAAV). J. Gene Med. *2*, 444–454.

36. Clark, K.R., Liu, X., McGrath, J.P., and Johnson, P.R. (1999). Highly purified recombinant adeno-associated virus vectors are biologically active and free of detectable helper and wild-type viruses. Hum. Gene Ther. *10*, 1031–1039.

37. Qu, G., Bahr-Davidson, J., Prado, J., Tai, A., Cataniag, F., McDonnell, J., Zhou, J., Hauck, B., Luna, J., Sommer, J.M., et al. (2007). Separation of adeno-associated virus type 2 empty particles from genome containing vectors by anion-exchange column chromatography. J. Virol. Methods *140*, 183–192.

38. Kaludov, N., Handelman, B., and Chiorini, J.A. (2002). Scalable purification of adeno-associated virus type 2, 4, or 5 using ion-exchange chromatography. Hum. Gene Ther. *13*, 1235–1243.

39. Okada, T., Nonaka-Sarukawa, M., Uchibori, R., Kinoshita, K., Hayashita-Kinoh, H., Nitahara-Kasahara, Y., Takeda, S., and Ozawa, K. (2009). Scalable purification of adeno-associated virus serotype 1 (AAV1) and AAV8 vectors, using dual ion-exchange adsorptive membranes. Hum. Gene Ther. *20*, 1013–1021.

40. Lock, M., Alvira, M.R., and Wilson, J.M. (2012). Analysis of particle content of recombinant adeno-associated virus serotype 8 vectors by ion-exchange chromatography. Hum. Gene Ther. Methods *23*, 56–64.

41. Davidoff, A.M., Ng, C.Y.C., Sleep, S., Gray, J., Azam, S., Zhao, Y., McIntosh, J.H., Karimipoor, M., and Nathwani, A.C. (2004). Purification of recombinant adeno-associated virus type 8 vectors by ion exchange chromatography generates clinical grade vector stock. J. Virol. Methods *121*, 209–215.

42. Fu, X., Chen, W.C., Argento, C., Clarner, P., Bhatt, V., Dickerson, R., Bou-Assaf, G., Bakhshayeshi, M., Lu, X., Bergelson, S., and Pieracci, J. (2019). Analytical strategies for quantification of adeno-associated virus empty capsids to support process development. Hum. Gene Ther. Methods *30*, 144–152.

43. Wang, C., Mulagapati, S.H.R., Chen, Z., Du, J., Zhao, X., Xi, G., Chen, L., Linke, T., Gao, C., Schmelzer, A.E., and Liu, D. (2019). Developing an Anion Exchange Chromatography Assay for Determining Empty and Full Capsid Contents in AAV6.2. Mol. Ther. Methods Clin. Dev. *15*, 257–263.

44. Sommer, J.M., Smith, P.H., Parthasarathy, S., Isaacs, J., Vijay, S., Kieran, J., Powell, S.K., McClelland, A., and Wright, J.F. (2003). Quantification of adeno-associated virus particles and empty capsids by optical density measurement. Mol. Ther. *7*, 122–128.

45. Moço, P.D., Aharony, N., and Kamen, A. (2020). Adeno-associated viral vectors for homology-directed generation of CAR-T Cells. Biotechnol. J. *15*, e1900286.

46. Urabe, M., Xin, K.Q., Obara, Y., Nakakura, T., Mizukami, H., Kume, A., Okuda, K., and Ozawa, K. (2006). Removal of empty capsids from type 1 adeno-associated virus vector stocks by anion-exchange chromatography potentiates transgene expression. Mol. Ther. *13*, 823–828.

47. Stanton, D. (2019). BIA separations providing chromatography columns to AveXis. BioProcess Insider, https://bioprocessintl.com/bioprocess-insider/upstream-downstream-processing/bia-separations-providing-chromatography-columns-for-avexis.

48. Dickerson, R., Argento, C., Peracci, J., and Bakhshayeshim, M. (2020). Separating empty and full rAAV particles using isocratic anion exchange chromatography. Biotechnol. J. *16*, e2000015.

49. Carta, G., and Jungbauer, A. (2010). Protein Chromatography: Process Development and Scale-up, First Edition (Wiley-VCH), pp. 85–122.

50. Harinarayan, C., Mueller, J., Ljunglöf, A., Fahrner, R., Van Alstine, J., and van Reis, R. (2006). An exclusion mechanism in ion exchange chromatography. Biotechnol. Bioeng. *95*, 775–787.

51. Fóti, G., Révész, G., Hajós, P., Pellaton, G., and Sz Kováts, E. (1996). Classical retention mechanism in ion exchange chromatography. Theory and experiment. Anal. Chem. *68*, 2580–2589.

52. Geldart, R.W., Yu, Q., Yu, Q., Wankat, P.C., and Wang, N.H.L. (1986). Improving elution and displacement ion-exchange chromatography by adjusting eluent and displacer affinities. Sep. Sci. Technol. *21*, 873–885.

53. Yamamoto, S., Nakanishi, K., and Matsuno, R. (1998). Ion-Exchange Chromatography of Proteins (Marcel Dekker), pp. 36–78.

54. Joshi, P.R.H., Cervera, L., Ahmed, I., Kondratov, O., Zolotukhin, S., Schrag, J., Chahal, P.S., and Kamen, A.A. (2019). Achieving high-yield production of functional AAV5 gene delivery vectors via fedbatch in an insect cell-one baculovirus system. Mol. Ther. Methods Clin. Dev. *13*, 279–289.

55. Chahal, P.S., Schulze, E., Tran, R., Montes, J., and Kamen, A.A. (2014). Production of adeno-associated virus (AAV) serotypes by transient transfection of HEK293 cell suspension cultures for gene delivery. J. Virol. Methods *196*, 163–173.

56. Schuck, P. (2000). Size-distribution analysis of macromolecules by sedimentation velocity ultracentrifugation and lamm equation modeling. Biophys. J. *78*, 1606–1619.

57. Brautigam, C.A. (2015). Calculations and publication-quality illustrations for analytical ultracentrifugation data. Methods Enzymol. *562*, 109–133.